Imaging the pair-correlated excitation function: The F + CH 4 HF (v)+ CH 3 (=0) reaction

Weicheng Shiu, Jim J. Lin, Kopin Liu, Malcom Wu, and David H. Parker

---

Articles you may be interested in

Rotationally selected product pair correlation in F + CD 4 DF ( )+ CD 3 (=0, N)
J. Chem. Phys. **120**, 5863 (2004); 10.1063/1.1689634

Mode-correlated product pairs in the F + CHD 3 DF + CHD 2 reaction
J. Chem. Phys. **119**, 8289 (2003); 10.1063/1.1611877

Photodetachment of F (H 2 O) n (n=1–4): Observation of charge-transfer states [F (H 2 O) n +] and the transition state of F+H 2 O hydrogen abstraction reaction
J. Chem. Phys. **115**, 2889 (2001); 10.1063/1.1394758

Energy-dependent cross sections and nonadiabatic reaction dynamics in F (2 P 3/2 , 2 P 1/2)+n– H 2 HF (v,J)+ H
J. Chem. Phys. **111**, 8404 (1999); 10.1063/1.480182

Rotationally resolved differential scattering cross sections for the reaction F+para-H 2 (v=0,j=0) HF (v =2,3,j)+ H
J. Chem. Phys. **110**, 10231 (1999); 10.1063/1.478955
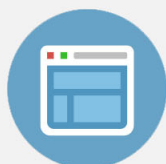
Imaging the pair-correlated excitation function: The $F+CH_4 \rightarrow HF(v')$ $+CH_3(\nu=0)$ reaction

Weicheng Shiu, Jim J. Lin,[a] and Kopin Liu[b]
Institute of Atomic and Molecular Sciences, Academia Sinica P.O. Box 23-166, Taipei 106, Taiwan

Malcom Wu and David H. Parker
Department of Molecular and Laser Physics, University of Nijmegen, Toernooiveld 1, 6525 ED Nijmegen, The Netherlands

The velocity map ion imaging technique was applied to measure the reaction excitation function for the first time. It was found that the "raw" excitation function was significantly distorted by the density-to-flux transformation of the title reaction. Through a systematic investigation, possible reasons for such a dramatic effect are outlined. In addition, the state-resolved, pair-correlated excitation functions and branching ratios are presented. Effects of imperfect time slicing in the time-sliced velocity imaging technique in general are also discussed. © *2004 American Institute of Physics.* [DOI: 10.1063/1.1629668]

I. INTRODUCTION

The reactive excitation function $\sigma(E_c)$, namely the dependence of the integral cross section (ICS) on the initial translational energy E_c, is an important quantity in reaction dynamics. It measures the efficiency of the translational energy in driving the reaction system to the critical region of the transition state. It also serves as the most direct link between reaction dynamics and thermal kinetics.[1] The crossed molecular beam method has long been established to be one of the most powerful approaches for such investigations.[1,2]

Over the past several decades, we have examined the state-specific excitation functions for a number of elementary reactions[1] and energy transfer processes,[3] using a rotating sources, crossed-beam apparatus. The product state specificity was achieved by either laser-induced fluorescence or resonance-enhanced multiphoton ionization (REMPI) for interrogation. Because the density-to-flux problem—which is associated with the laser based detection scheme and requires the differential cross section (DCS) information—is of concern, a simpler experimental approach to alleviate the problem for obtaining the excitation function was developed.[4] The premise of this approach relies on the fact that the true cross section is independent of the experimental geometry. Practically, we varied the collision energy by changing the intersection angle of the two molecular beams. Using two different seeding mixtures for the radical beam, thus two different beam speeds or kinematics for the same E_c, we examined the consistency of these two sets of data over the overlapped energy range. This approach has stood the test for many reactions, and appears to be quite reliable.[1,5–7]

The above-mentioned approach, however, makes no explicit correction for the density-to-flux problem. The consistency criterion provides a necessary, but not a sufficient condition to recover the excitation function from measurements. Reported here is a case where the previous approach can lead to a very different impression of the excitation function of interest. Shown in Fig. 1 is the "raw" or the "apparent" excitation function, acquired in the same manner as the previous investigations,[1,4] of the title reaction for the formation of the ground state $CH_3(\nu=0)$. The F-atom beam was generated by discharging 5% F_2 seeded either in He or in Ne with the beam speed of 1.62 or 1.13 km/s, respectively. The former covers the energy range from 1.7 to 7.3 kcal/mol, whereas the latter from 0.48 to 4.9 kcal/mol. As is seen, the consistency of the two sets of data over the overlapped energy range is quite reasonable. The shape of the apparent excitation function is, however, peculiar. It rises sharply from the threshold of <0.5 kcal/mol and forms a prominent peak near 1.3 kcal/mol followed by a rapid decline with further increase in collision energy. Particularly worth noting are how abrupt the post-maximum decline is and how small the cross section approaches at high energies. Its appearance also differs significantly from those found previously for the isotopically analogous reaction of $F+CD_4$.[8] This "unusual" shape prompted us to scrutinize the title reaction further and to examine the effects of the density-to-flux transformation on the ICS measurements in greater detail.

The remainder of the paper is organized as follows: A brief description about the experiments will be given in Sec. II. The results will then be presented, which include the effectiveness of time slicing in the three-dimensional (3D) velocity imaging and the effects of the density-to-flux transformation on ICS. A discussion of the dynamical implications of the excitation function will then follow. The reason for the failure of the previous approach (Fig. 1) will also be discussed; this should serve as a caution for future investigations.

[a]Also at: Department of Applied Chemistry, National Chiao Tung University, Hsinchu, Taiwan 300. Electronic mail: jimlin@po.iams.sinica.edu.tw
[b]Also at: Department of Chemistry, National Taiwan Normal University, Taipei 106, Taiwan. Electronic mail: kpliu@gate.sinica.edu.tw
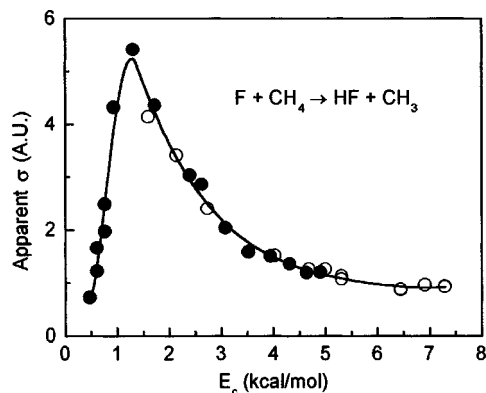
FIG. 1. The apparent excitation function for the formation of $CH_3(v=0)$ product from the $F+CH_4$ reaction. Two different F-atom beams, 5% F_2 seeded in He (○) and 5% F_2 in Ne (•), were used to cover the full energy range.

II. EXPERIMENT

The experiment was carried out using the rotating-sources, crossed-beam apparatus as detailed previously.[8–10] The probe of the CH_3 product was achieved by a $(2+1)$ REMPI scheme via the intermediate $3p_z$ $^2A''$ Rydberg state.[8,11] For the "apparent" excitation function measurement (Fig. 1), the ion optics was operated in the spatial mode, namely no velocity mapping, to minimize the local bleaching effects on the microchannel plates from long-term running. At each intersection angle the probe laser wavelength, near 333 nm, was scanned over the Q-head of the $CH_3(0_0^0)$ band, and the ion signal was acquired by a boxcar integrator gated for $m/e=15$ in the ion time-of-flight (TOF) mode of operation. Dividing the signal by the initial relative speed yields the "apparent" cross section.

To recover the true excitation function, one needs to make the density-to-flux correction, which in turn requires information about DCSs over a fairly wide range of energies. Performing the same experiments but shifting to the time-sliced velocity-imaging mode of operation[10] for different collision energies accomplished this. To make direct comparisons to the "boxcar" results (Fig. 1), the laser was scanning back and forth over the Q branch many times while the image was acquired. The scanning of the laser wavelengths results in an approximately rotationally integrated image for a given vibrational state of CH_3 products, which is different from the partially rotational-selected image reported previously for the $F+CD_4$ reaction.[10,12,13] No rotational alignment effects were found, even when the N-selected CH_3 (and CD_3) products were imaged (unpublished results). To make the density-to-flux transformation more robust, the path of the probe laser was also scanned (typically ± 8 mm) back and forth to generate an artificial laser sheet for interrogation.[10] Again, the consistency criterion that the ICS measurements at the same collision energy should be independent of the experimental geometries was examined to ensure the results are devoid of experimental artifacts.

III. RESULTS

A. Effects of time slicing

For a scattering or a photodissociative process, the desired differential quantity is $d^3\sigma/du\,d\Omega$, where $d\Omega$ is the solid angle element $d(\cos\theta)d\varphi$ in the center-of-mass (c.m.) frame. Using the 3D velocity mapping approach, either the Doppler-selected TOF method[14] or the time-sliced velocity imaging technique,[10] one actually measures $d^3\sigma/du_x\,du_y\,du_z$ or $D(u_x, u_y, u_z)$ in a c.m. Cartesian coordinate after the density-to-flux correction. Since the c.m. velocity volume element should be invariant to the coordinates, i.e., Cartesian or polar, the desired and the measured quantities can readily be related through $d^3\sigma/u^2\,du\,d\Omega = d^3\sigma/du_x\,du_y\,du_z$. Since the scattering process usually exhibits a cylindrical symmetry around the initial relative velocity vector, one is free to integrate the azimuthal angle to just report the DCS as $d^2\sigma/du\,d(\cos\theta)\propto u^2\,D(u_x, u_y, u_z \approx 0)$,[14] where the z axis denotes the ion TOF axis in the time-sliced velocity imaging approach. And $D(u_x, u_y, u_z \approx 0)$ can be approximated by the velocity mapped image (in the $x-y$ plane which contains the relative velocity) when the Newton sphere is sliced through the center. Practically, this simple relationship between the measured and desired quantities will be valid only if the gate width used in the time-sliced, velocity-mapped image is sufficiently narrow to have an effective central slicing. Clearly, given a gate width, there is always a range of u, for which the products are recoiled with sufficiently small velocities so that the slicing condition cannot be met. The situation then returns to the conventional two-dimensional (2D) (or compressed) imaging. The questions are: How narrow a gate width should one use for effective time slicing? And, how can corrections be made for imperfect slicing when measuring very small values of u?

Figure 2 shows the systematic study of the effects of the gate width. The initial collision energy was 4.91 kcal/mol, and the voltages of the ion optics were held constant (14 V/cm extraction field) while the gate width was varied. Figures 2(a)–2(c) display three representative images corresponding to the narrow, medium, and wide gates, respectively. Three well-separated rings are clearly visible. Energetically, they are ascribed to the coincidently formed HF products in $v=3$, 2, and 1, respectively. At first glance, it might be surprising to see such well-separated features for the wide-gate case [Fig. 2(c)]. After all, if the gate is wide enough, then the image should essentially become a compressed (2D) one—blurring the structural features should be observed. The main reason is in fact the very same as the need for the density-to-flux transformation.[4] In a typical crossed-beam experiment, the time for collision is long, $>5-10$ μs depending on the molecular beam pulse widths. The probe laser samples only those products remaining in the laser illumination region when it is fired, and thus are blind to those flying out of the probing volume. In other words, the laser (sheet) detection effectively acts as a first-cut (spatial) slice in the scattering zone.

Summing up the ion counts within the annulus for each individual ring yields the total ion signals for the corresponding pair-correlated product states. The results are summa-
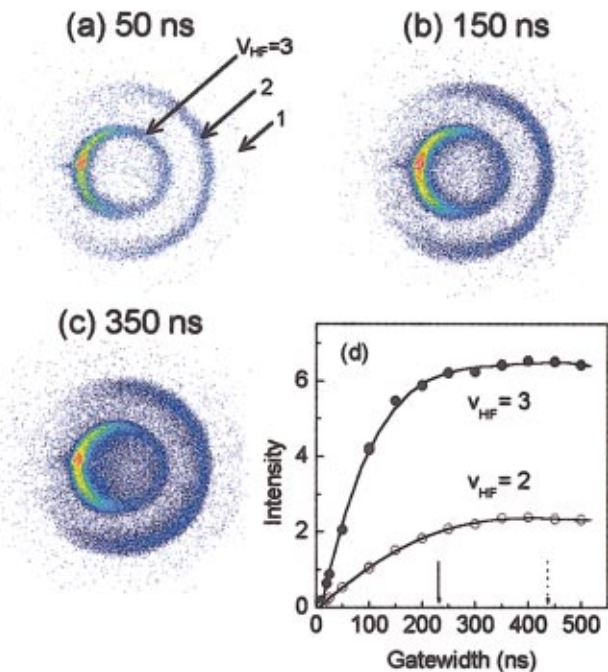
FIG. 2. (Color) Exemplified in (a)–(c) are the raw images taken with three different gate widths for slicing. The collision energy is 4.91 kcal/mol. The results are summarized in (d) which shows how the signal for the correlated HF-vibration state depends on the gate width used. The arrows mark the calculated temporal spreads of the ion clouds for $v_{HF}=3$ ($\downarrow$) and $v_{HF}=2$ ($\downarrow$).

FIG. 3. The normalized fluxes into $v_{HF}=3$ (•) and $v_{HF}=2$ (○) product states at $E_c=4.91$, 2.63, and 1.73 kcal/mol, respectively. The normalization is performed by dividing the experimentally derived "flux" by either the gate width or the temporal spread, whichever is smaller. The fluxes for the three energies are not related to one another.

rized in Fig. 2(d). [The events for HF($v=1$) are statistically negligible in this work.] Also marked in arrows are the maximal temporal spreads of the corresponding pairs, calculated on energetic grounds and the ion-optics settings. The signals display a linear rise for smaller gate width, and gradually approach their respective limits at different rates for wider gates. Similar experiments were also performed at two lower collision energies 2.63 and 1.73 kcal/mol. The general observations noted in Fig. 2(d) appear to be universal. All of these can readily be understood. It should also be apparent that the figure-of-merit for the effectiveness of time slicing has to do with the ratio of the gate width and the temporal spread of the ion clouds. Qualitatively, an ion cloud with a small temporal spread will require a narrower gate. In addition, the rate of approaching the limit depends on, among other factors, the actual angular distribution.

With a series of images as a function of gate widths in hand, we are in a position to answer the first question addressed above. For each image, we performed the density-to-flux transformation as detailed previously.[10] It should be noted that the generation of the density-to-flux transformation matrix was based on the assumption that the gate width is narrow enough to have a valid sliced image. If the gate width is too wide, the (blind) use of the matrix will yield an erroneous result. Hence, our strategy is to use the gate width evolution of various dynamics attributes as a gauge to find out the optimal gate width to be used. Figure 3 summarizes the results for the reactive fluxes into HF($v=3$) and HF($v=2$), and Fig. 4 for their ratios at $E_c=4.91$, 2.63, and 1.73 kcal/mol, respectively. (The state-resolved, pair-correlated DCS is too involved and will be the subject for the future.)
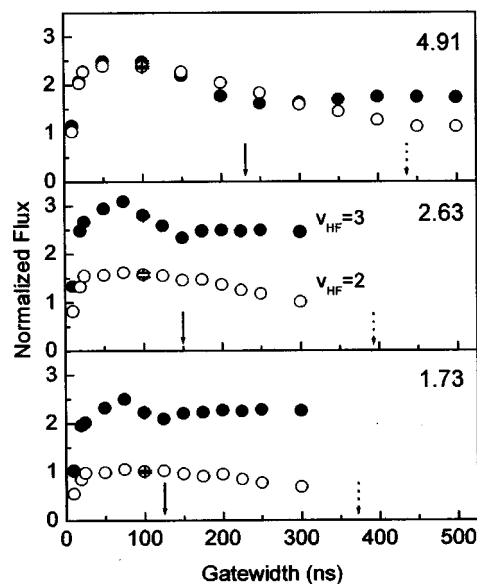
To account for the fact that the narrower gate inevitably samples few events, we normalized the state-resolved fluxes in Fig. 3 by either the gate width used or the corresponding temporal spread of the ion cloud, whichever is smaller. The sharp decrease of the normalized flux for gate width ≤ 25 ns is an experimental artifact, arising from the imperfect square-wave gating of the ICCD. The general trends are quite apparent: *A too-wide gate will underestimate the reactive flux and will make the branching ratio $(v'=3)/(v'=2)$ smaller than it should be.* The most critical parameter in deciding the gate width to be used is the relative magnitude of the gate width to the temporal spread of the smallest ring to be detected. An inspection of Figs. 3 and 4 indicates a ratio of $\leq 1/3$ as an empirical rule-of-thumb.
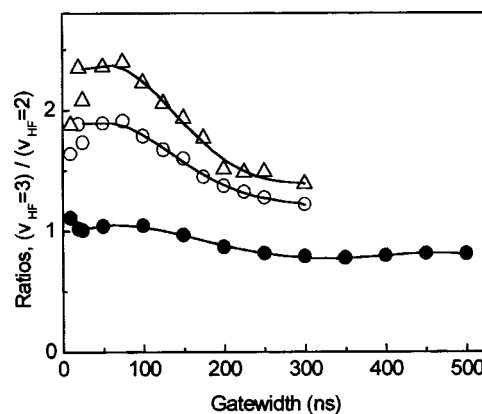

FIG. 4. Dependencies of the correlated product flux ratios on gate widths for $E_c=4.91$ (•), 2.63 (○), and 1.73 (△) kcal/mol, respectively.
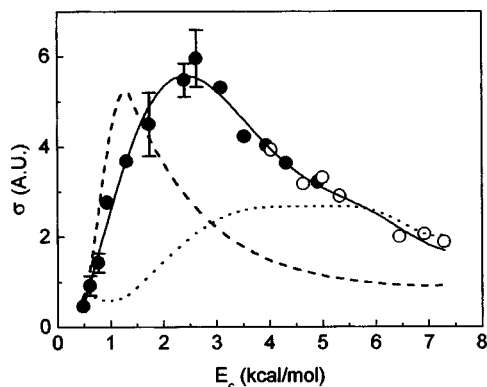
FIG. 5. The true excitation function obtained by the imaging approach. The closed circles were taken with the 5% F_2/Ne beam, and the open circles were with the 5% F_2/He beam. The error bars are the results from several independent measurements including the use of two different F-atom beams. The dashed line is the apparent excitation function taken from Fig. 1, and the dotted line gives the density-to-flux correction function (see the text for details). The solid line represented the "corrected" apparent excitation function.
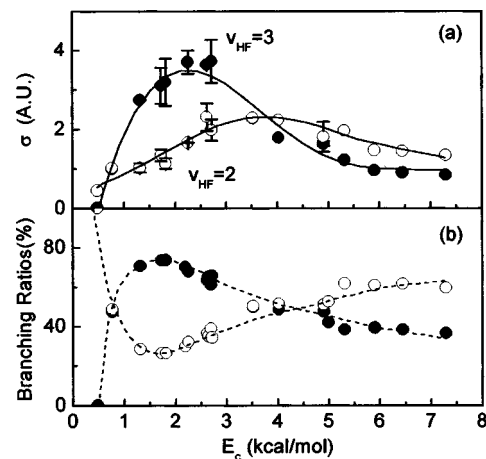

FIG. 6. In (a), the state-resolved, pair-correlated excitation functions of the title reaction are shown. Displayed in (b) are their branching ratios as a function of the collision energy.

B. Correction to the imperfect time slicing

As alluded to earlier, there are cases for which the recoil velocities of some products are too slow to be time-sliced effectively. This can often occur in the excitation function measurements. For example, the concomitant formation of HF($v=3$) is energetically closed at $E_c \lesssim 0.56$ kcal/mol when the CH$_3$($\nu=0$, low N) product is probed. Thus, near the pair-specific threshold region the rings for HF($v'=3$) will be quite small. Even the narrowest gate (10 ns) of a typical ICCD cannot perform time slicing for them. One is essentially back to the conventional 2D→3D backtransformation for those (very) slowly recoiled products. The correction to the imperfect time slicing is analogous to the wide gate results shown in Figs. 3 and 4. As is seen, the correction factor could be as large as a factor of 2 depending on the quantity, which in turn depends on the actual angular distribution. Alternatively, with the time-sliced velocity imaging technique, one can zoom in the image region of interest by lowering the voltages of the ion-optics setup.[10] In any event, those very slowly recoiled products usually represent only a very small fraction of total reactive fluxes—thus have little impact on ICS.

C. The "true" excitation function

Putting all together, we can now recover the excitation function. Experimentally, for each E_c two back-to-back images were acquired—one for the narrow gate (typically 30–50 ns) and the other for the wide gate (typically 350 ns). To normalize the narrow gate images (each acquired for about 3000 s) for different E_c's, a set of wide gate images (each acquired for 300 s) over the collision energy range was taken independently to minimize the long-term drift problems. After the density-to-flux transformation and the corrections to imperfect slicing of the narrow gate images, the resultant excitation function for the title reaction is shown in Fig. 5. For comparison, the "apparent" excitation function (Fig. 1) is also displayed here as the dashed line. The dra-

matic change in shapes—i.e., with versus without the density-to-flux transformation—is quite striking. More than ten images were taken under the identical beam geometries to those acquired by boxcar integrator (Fig. 1) over the energy range of 0.8–7.3 kcal/mol. The density-to-flux correction factor was obtained for each of these images. Connecting these correction factors yield the density-to-flux correction function, shown as the dotted line in Fig. 5. Applying this correction function to the "apparent" $\sigma(E_c)$ gives the corrected boxcar data, displayed as the solid line in Fig. 5. It is gratifying to see that it is entirely consistent with the true $\sigma(E_c)$ obtained by the imaging approach.

D. State-resolved, pair-correlated $\sigma(E_c)$ and branching ratios

Exemplified by Figs. 3 and 4 at three energies, Fig. 6 shows how the state-specific $\sigma(E_c)$ for CH$_3$($\nu=0$) is decomposed into the pair-correlated excitation functions [Fig. 6(a)] and how the correlated vibrational branching varies with the collision energy [Fig. 6(b)]. Figure 6 represents the first correlated quantity that has ever been measured over a wide range of collision energies in such detail for any chemical reaction.[13] The threshold for the formation of HF($v=3$), in concomitance with CH$_3$($\nu=0$), is ~0.56 kcal/mol. At low collision energies, HF($v=2$) dominates. But, once the HF($v=3$) channel opens up, its cross section rises rapidly and becomes the favored channel. At even higher energies, the cross sections for HF($v=3$) declines at a faster rate than $v=2$, and the two vibrational states become comparable with slight preference for HF ($v=2$). As a result, the peak of $\sigma(E_c)$ shown in Fig. 5 arises predominantly from the behavior of HF($v=3$). The formation of the more exoergic channel, HF($v=1$), is always small even at the highest collision energy of this study. Since there are practically only two state-correlated channels, the branching ratios of HF($v=3$) and HF($v=2$) display an almost perfect anticorrelation with collision energies as seen in Fig. 6(b).

We note in passing that the results shown in Fig. 6 are not inconsistent with the previous bulb experiments,[15–17] for

which HF($v=2$) was found to be the most populated state. Under the thermal conditions, the collision energy is low and with a wider distribution, thus the results will be dominated by the low energy collisions.

IV. DISCUSSION AND CONCLUSION

The appearance of the true excitation function (Fig. 5) deserves some comments. The excitation function displays a fast rise near the threshold region and reaches a maximum, followed by a rapid decline with further increase in collision energy. Similar dependence of the cross section for the reaction $K+CH_3I \rightarrow KI+CH_3$ was reported by Gersh and Beinstein about 30 years ago,[18] so as for a number of other elementary reactions later.[2,19–21] Several dynamical models of hard-sphere variants have been proposed to rationalize the results, particularly on the post-maximum decline.[2,21] It is difficult to judge the validity of those empirical models because of the lack of reliable potential energy surface and more rigorous dynamic treatments. Consider two textbook examples:[22] the venerable line-of-center model of a hard sphere reaction, and a barrierless reaction governed by an attractive potential. The observed excitation function for F+CH₄ exhibits the characteristic of both models— resembling the former model for $E_c \lesssim 2.5$ kcal/mol and the latter one at higher energy. This seems to suggest a potential having a (early) barrier of ~ 0.5 kcal/mol to reaction and an attractive potential well after the transition state. The former is in accordance with the activation energy of 0.43 kcal/mol from the most recent thermal kinetics measurement.[23] As to the latter, it remains to be seen if the hydrogen bonding[24] of F–H···CH₃ in the exit channel alone is sufficient to provide the necessary attractive potential. The shapes of the state-correlated excitation function shown in Fig. 6(a) qualitatively support the proposed scenario. From the vibrationally adiabatic viewpoint, the reaction cross section of the least exoergic channel, $v_{HF}=3$, is expected to be influenced more by the attractive well in the post-threshold region than the $v_{HF}=2$ channel. Indeed, the pair-correlation excitation function for $v_{HF}=3$ displays a significantly faster decline after the peak.

Of course, it will be too unrealistic at this stage to believe that the dynamics of excitation function is governed by the proposed hybrid model. Here we merely wish to point out the subtle role the attractive interaction in the post-barrier region might play for an earlier barrier reaction. The correlated vibrational branching ratios shown in Fig. 6 exhibit a complicated dependency on collision energies. This quantity in general depends, among other factors such as the geometry/motion of the transition state etc.,[12,13] sensitively on how steep the repulsive energy release is when the paired products depart. Further information on the potential energy surface and theoretical efforts is needed to quantitatively account for the results of Figs. 5 and 6.

We have elucidated above in detail how the density-to-flux transformation can alter the excitation function of the title reaction in a dramatic way. We have also investigated in practical ways how to properly choose the gate width in a time-sliced velocity imaging experiment, and how to esti-

mate the correction factors should the circumstances force one back to the 2D image mode. A vital question remains to be addressed: Why does the previous approach outlined in Sec. I, which apparently works reasonably well for many other systems, fail so badly for the present reaction?

There is no doubt that the answer to the question is complicated. In the end, we believe that to a large extent it has to do with the highly quantized nature of the DCS, $d^2\sigma/dud(\cos\theta)$, of the present reaction. The title reaction is very exoergic, $\Delta H_0^0 = -31.85$ kcal/mol. Energetically, numerous rovibrational states of HF coproducts can be formed. The kinematic and dynamic constraints, however, channel most of products into only a small subset of available product states. Moreover, the most populated HF-product vibrational states are the two least exoergic ones, which results in a highly biased probe in the density mode because of the large disparities of the u^2 term in going from the probed density to the reactive flux in the c.m. velocity space. The last point is precisely the dominant reason for the appearance of the density-to-flux correction function (the dotted line in Fig. 5) that underlies the dramatic changes seen from Fig. 1 to Fig. 5. The highly anisotropic angular distributions of the two rings, as revealed from images shown in Fig. 2, compound the effects further.

It is a bit frustrating to find out that in order to obtain the dynamical information about ICS for a scattering process, one first needs to know about the more detailed DCS. Nevertheless, the take-home lesson from this study is that it pays off to examine the DCS data, at least at a few representative collision energies, to ensure the obtained ICS results are not distorted too far from the truth.

[1] K. Liu, Int. Rev. Phys. Chem. **20**, 189 (2001).
[2] A. Gonzalez Urena, J. Phys. Chem. **96**, 8212 (1992); Adv. Chem. Phys. **66**, 213 (1987).
[3] K. Liu, R. G. MacDonald, and A. F. Wagner, Int. Rev. Phys. Chem. **9**, 187 (1990).
[4] D. M. Sonnenfroh and K. Liu, Chem. Phys. Lett. **176**, 183 (1991).
[5] W. D. Geppert, D. Reignier, T. Stoecklin, C. Naulin, M. Costes, D. Chastaing, S. D. Le Picard, I. R. Sims, and I. W. M. Smith, Phys. Chem. Chem. Phys. **2**, 2873 (2000).
[6] C. Naulin and M. Costes, Chem. Phys. Lett. **310**, 231 (1999).
[7] W. D. Geppert, C. Naulin, and M. Costes, Chem. Phys. Lett. **333**, 51 (2001); **364**, 121 (2002).
[8] J. Zhou, J. J. Lin, W. Shiu, S.-C. Pu, and K. Liu, J. Chem. Phys. **119**, 2538 (2003).
[9] F. Dong, S.-H. Lee, and K. Liu, J. Chem. Phys. **113**, 3633 (2000).
[10] J. J. Lin, J. Zhou, W. Shiu, and K. Liu, Rev. Sci. Instrum. **74**, 2495 (2003).
[11] J. W. Hudgens, T. G. DiGiuseppe, and M. C. Lin, J. Chem. Phys. **79**, 571 (1983).
[12] J. J. Lin, J. Zhou, W. Shiu, and K. Liu, Science **300**, 966 (2003).
[13] J. Zhou, J. J. Lin, W. Shiu, and K. Liu, J. Chem. Phys. **119**, 4997 (2003).
[14] Y.-T. Hsu, K. Liu, L. A. Pederson, and G. C. Schatz, J. Chem. Phys. **111**, 7921 (1999).
[15] W. W. Harper, S. A. Nizkorodov, and D. J. Nesbitt, J. Chem. Phys. **113**, 3670 (2000).
[16] M. A. Nazar and J. C. Polanyi, Chem. Phys. **55**, 299 (1981).
[17] M. A. Wickramaaratchi, D. W. Setser, H. Hildebrandt, B. Korbitzer, and H. Heydtmann, Chem. Phys. **94**, 109 (1985).

[18] M. E. Gersh and R. B. Beinstein, J. Chem. Phys. **55**, 4661 (1971).

[19] J. M. L'Hermite, G. Ragmat, and R. Vetter, J. Chem. Phys. **95**, 3347 (1991).

[20] A. Gupta, D. S. Perry, and R. N. Zare, J. Chem. Phys. **72**, 6237 (1980).

[21] V. Saez Rabanos, E. Verdasco, V. J. Herrero, and A. Gonzalez Urena, J. Chem. Phys. **81**, 5725 (1984).

[22] R. D. Levine and R. B. Bernstein, *Molecular Reaction Dynamics and Chemical Reactivity* (Oxford University Press, Oxford, 1987), pp. 58–64.

[23] A. Persky, J. Phys. Chem. **100**, 689 (1996); Chem. Phys. Lett. **298**, 390 (1998).

[24] B.-Q. Wang, Z.-R. Li, D. Wu, X.-Y. Hao, R.-J. Li, and C.-C. Sun, Chem. Phys. Lett. **375**, 91 (2003).